Science Advances
AAAS

advances.sciencemag.org/cgi/content/full/5/5/eaav5490/DC1

Supplementary Materials for

Single-atom nanozymes

Liang Huang, Jinxing Chen, Linfeng Gan, Jin Wang*, Shaojun Dong*

*Corresponding author. Email: jin.d.wang@gmail.com (J.W.); dongsj@ciac.ac.cn (S.D.)

Published 3 May 2019, *Sci. Adv.* **5**, eaav5490 (2019)
DOI: 10.1126/sciadv.aav5490

This PDF file includes:

Fig. S1. The structures of cytocrome P450, horseradish peroxidase, and catalase and the corresponding active center.
Fig. S2. Morphology of the Zn-MOF precursor.
Fig. S3. Structure of the Zn-MOF precursor.
Fig. S4. FTIR spectra of FePc, Zn-MOF, and FePc@Zn-MOF.
Fig. S5. Morphology and structure of FeN_5 SA/CNF.
Fig. S6. Surface area and pore structure characterization.
Fig. S7. HRTEM images of FeN_5 SA/CNF.
Fig. S8. XPS and Mössbauer spectra of FeN_5 SA/CNF.
Fig. S9. Morphology and atomic structure of FeN_5 SA/CNF@800°C.
Fig. S10. Morphology and atomic structure of FeN_5 SA/CNF@1000°C.
Fig. S11. Morphology and atomic structure of FeN_4 SA/CNF.
Fig. S12. Morphology and atomic structure of MnN_5 SA/CNF.
Fig. S13. Morphology and atomic structure of CoN_5 SA/CNF.
Fig. S14. Morphology and atomic structure of NiN_5 SA/CNF.
Fig. S15. Morphology and atomic structure of CuN_5 SA/CNF.
Fig. S16. UV-vis absorption spectra of the catalysts.
Fig. S17. Oxidase-like activities of FeN_5 SA/CNF in different conditions.
Fig. S18. UV-vis absorption spectra of FeN_5 SA/CNF.
Fig. S19. Morphology and structure of synthesized conventional nanozymes.
Fig. S20. UV-vis absorption spectra of TMB solutions.
Fig. S21. Morphological changes in bacteria.
Fig. S22. In vitro cytotoxicity experiments.
Fig. S23. Photographs of in vivo mice wound model.
Fig. S24. Double-reciprocal plots of activity of these catalysts.
Fig. S25. The analysis of the intermediate state of and active center in FeN_5 SA/CNF.
Fig. S26. Theoretical investigation of oxidase-like activity.
Table S1. Mössbauer parameters of FeN_5 SA/CNF.
Table S2. Comparison of oxidase-like activity of synthesized catalysts.

Table S3. Comparison of the kinetic constants of the single-atom enzyme mimics.
Table S4. The adsorption energy on the single-atom catalysts.
Table S5. Reaction free energy of intermediate species on single-atom catalysts.
Table S6. Comparison of the kinetic constants of FeN_5 SA/CNF and nanozymes.
References (*44–51*)

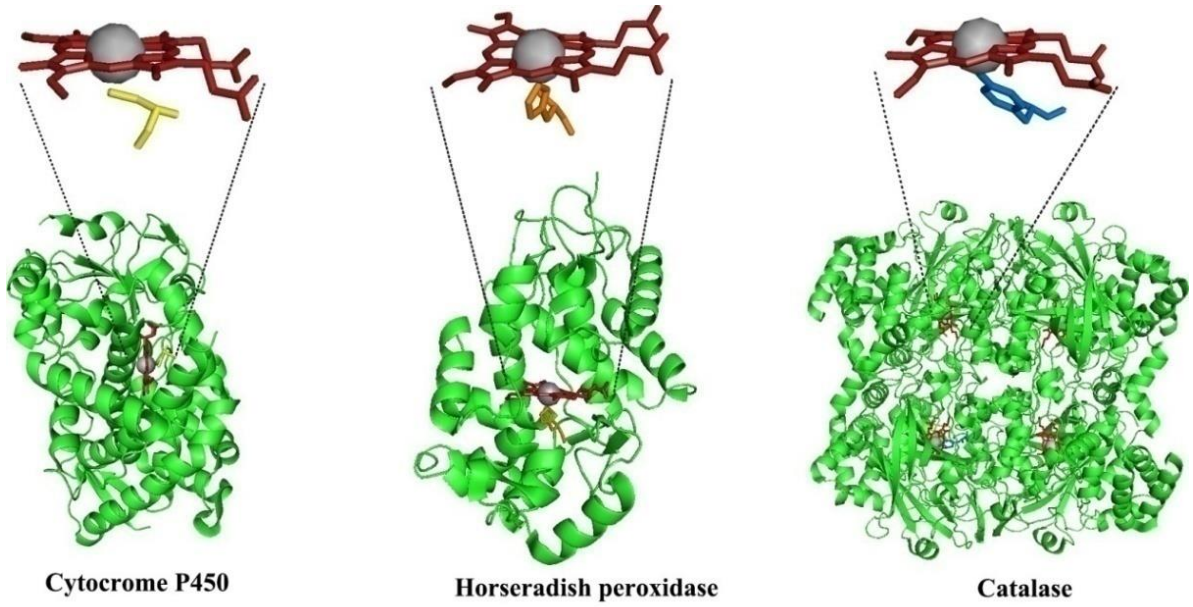

Fig. S1. The structures of cytocrome P450, horseradish peroxidase, and catalase and the corresponding active center. The active centers of these enzymes are heme coordinate with axial ligands of thiolate (cysteine), imidazole (histidine) and phenolic hydroxy (tyrosine), respectively.

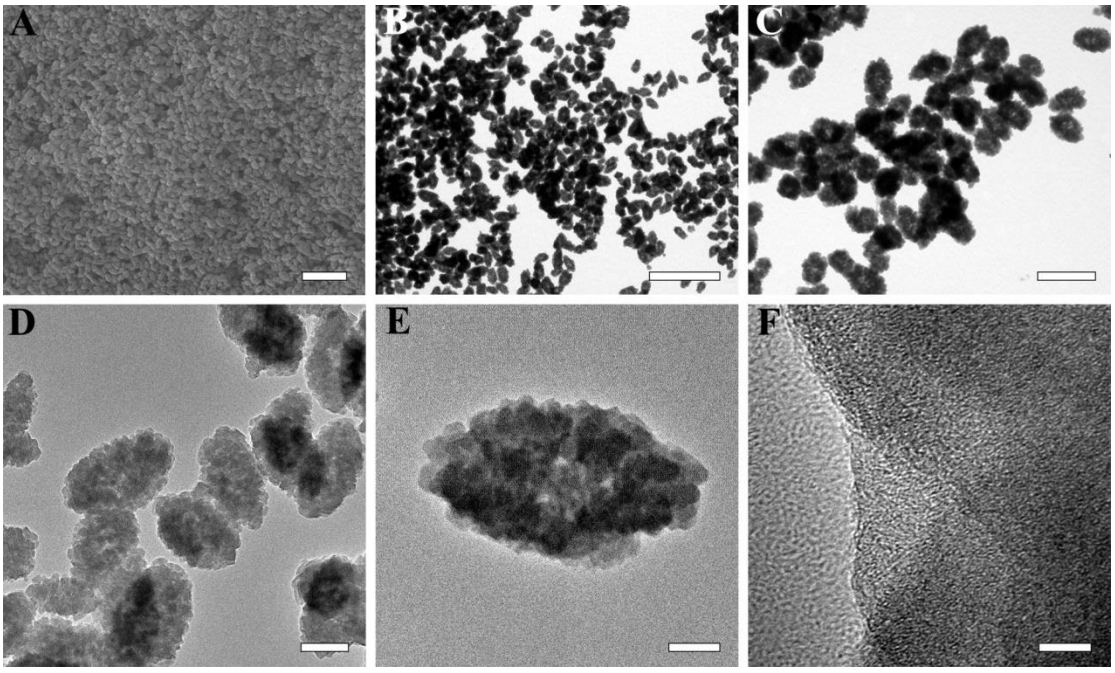

Fig. S2. Morphology of the Zn-MOF precursor. (A) SEM image and **(B)** TEM image of Zn-MOF. **(C, D)** TEM images and **(E, F)** HRTEM images of FePc@Zn-MOF. The scale bar in (A) 2 μm, (B) 2 μm, (C) 500 nm, (D) 200 nm, (E) 100 nm, (F) 5 nm.

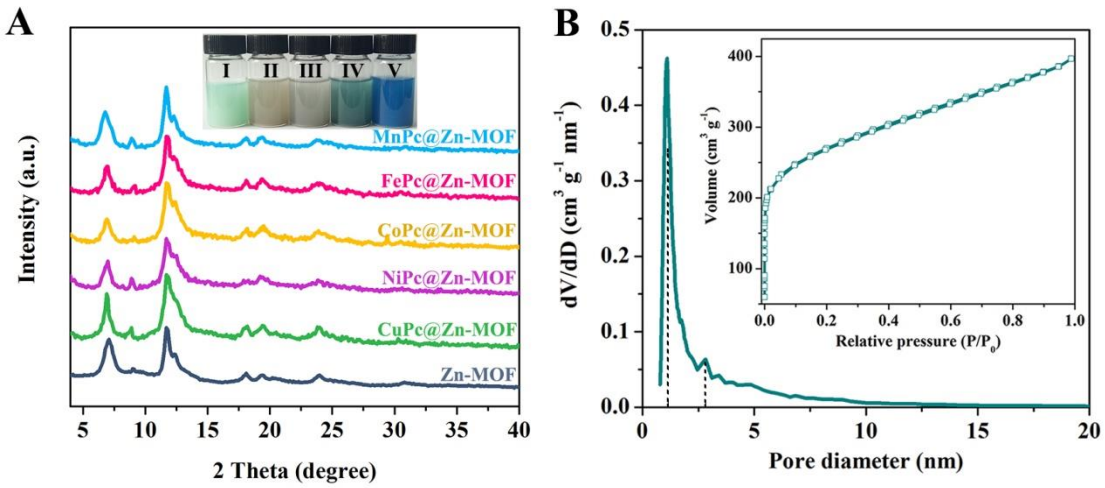

Fig. S3. Structure of the Zn-MOF precursor. (A) XRD pattern of MnPc@Zn-MOF (I), FePc@Zn-MOF (II), CoPc@Zn-MOF (III), NiPc@Zn-MOF (IV), CuPc@Zn-MOF (V) and Zn-MOF. Inset is the optical image of the corresponding MPc@Zn-MOF in ethanol solution (10 mg mL^{-1}). (Photo Credit: Liang Huang, Changchun Institute of Applied Chemistry) **(B)** Pore size distribution of FePc@Zn-MOF, and the inset of (B) is the corresponding N_2 adsorption/desorption isotherms.

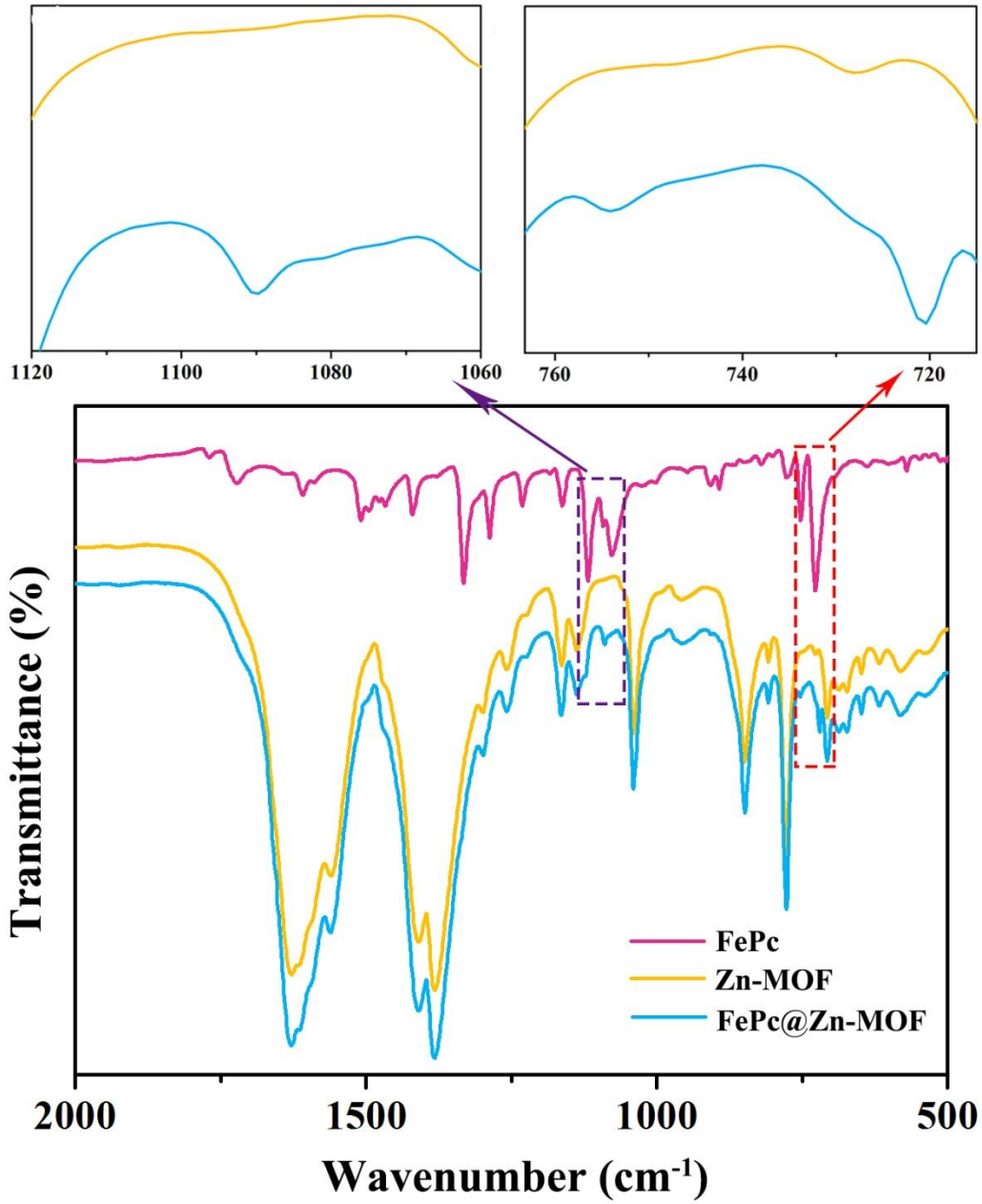

Fig. S4. FTIR spectra of FePc, Zn-MOF, and FePc@Zn-MOF. The intensity of the peaks in FePc@Zn-MOF at 1090 cm^{-1} (top left), 754 cm^{-1} and 721 cm^{-1} (top right) ascribed to the characteristic peaks of FePc indicated by dashed boxes.

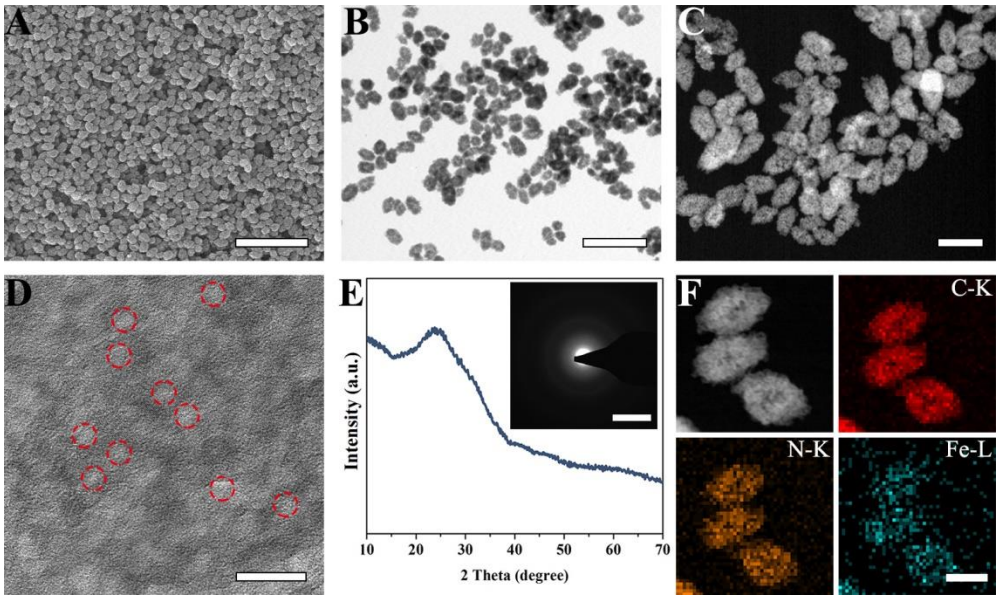

Fig. S5. Morphology and structure of FeN_5 SA/CNF. (A) SEM image, **(B)** TEM image, **(C)** STEM image, **(D)** HRTEM image, **(E)** XRD pattern and **(F)** TEM-EDS elemental mapping images of FeN_5 SA/CNF. The porous structure in (D) is indicated by circles. The inset of (E) is corresponding SAED pattern. The scale bar in (A) 2 μm, (B) 1 μm, (C) 500 nm, (D) 20 nm, inset (E) 5 nm^{-1}, (F) 200 nm.

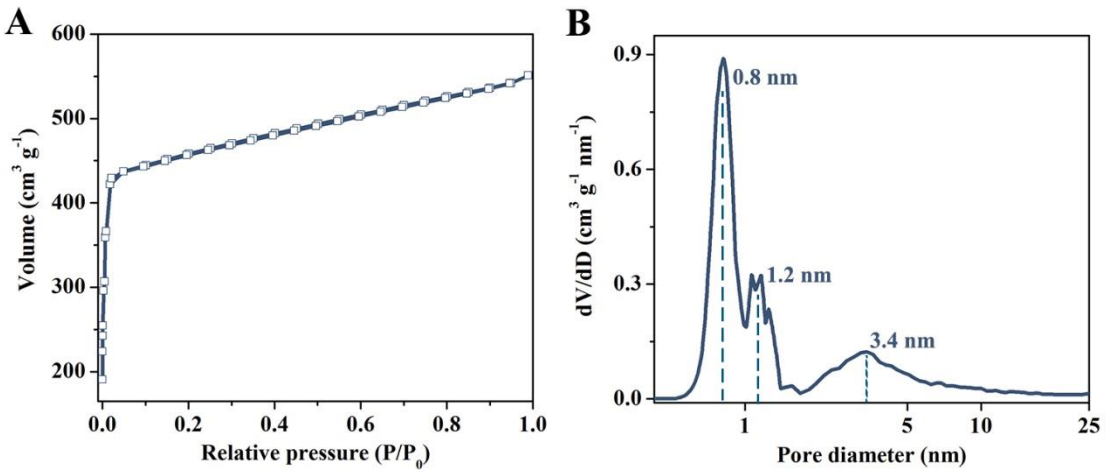

Fig. S6. Surface area and pore structure characterization. (A) N_2 adsorption/desorption isotherms and **(B)** pore size distribution of FeN_5 SA/CNF.

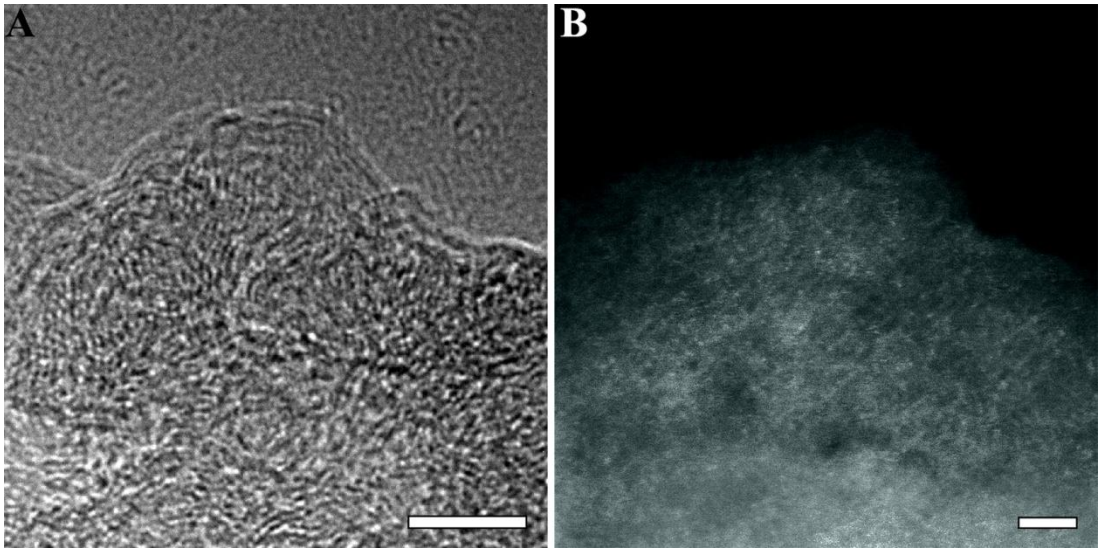

Fig. S7. HRTEM images of FeN_5 SA/CNF. (A) HRTEM image and **(B)** HAADF-STEM image of FeN_5 SA/CNF. The scale bar in (A) 5 nm, (B) 2 nm.

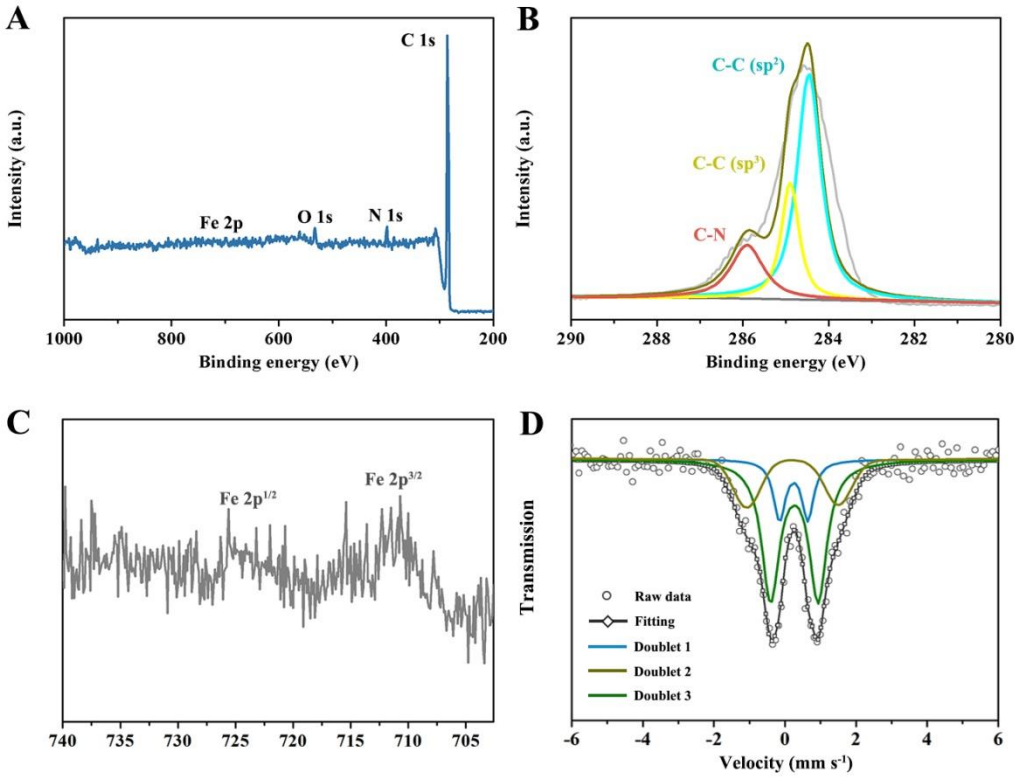

Fig. S8. XPS and Mössbauer spectra of FeN_5 SA/CNF. (A) XPS spectrum of FeN_5 SA/CNF, and the corresponding high resolution XPS spectra of **(B)** C 1s and **(C)** Fe 2p. **(D)** ^{57}Fe Mössbauer spectrum of FeN_5 SA/CNF.

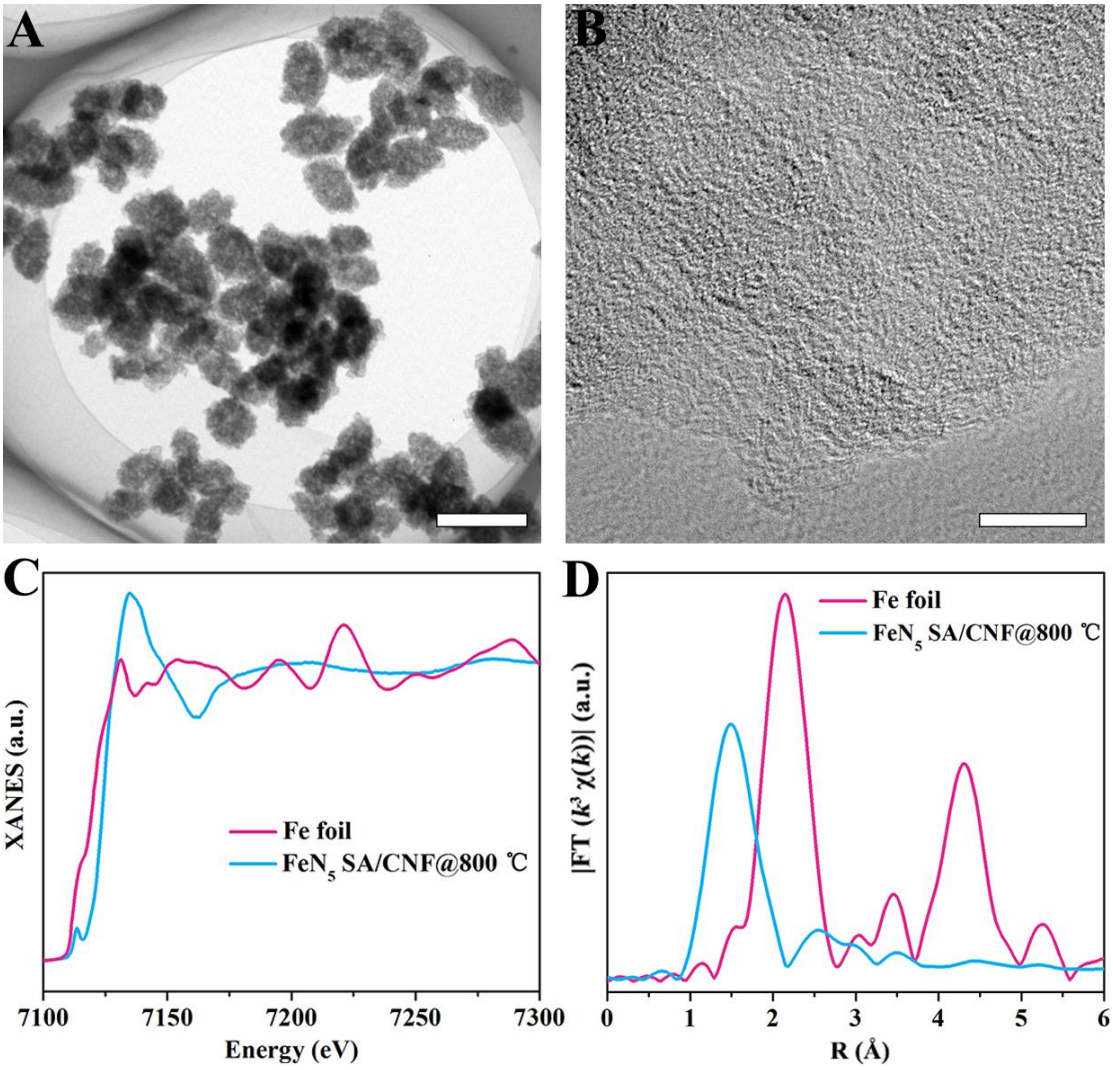

Fig. S9. Morphology and atomic structure of FeN_5 SA/CNF@800°C. (A) TEM image and **(B)** HRTEM image of FeN_5 SA/CNF@800 °C. **(C)** Normalized XANES spectra at Fe K-edge of the Fe foil and FeN_5 SA/CNF@800°C, and the corresponding **(D)** k^3-weighted Fourier transform spectra. The scale bar in (A) 500 nm, (B) 5 nm.

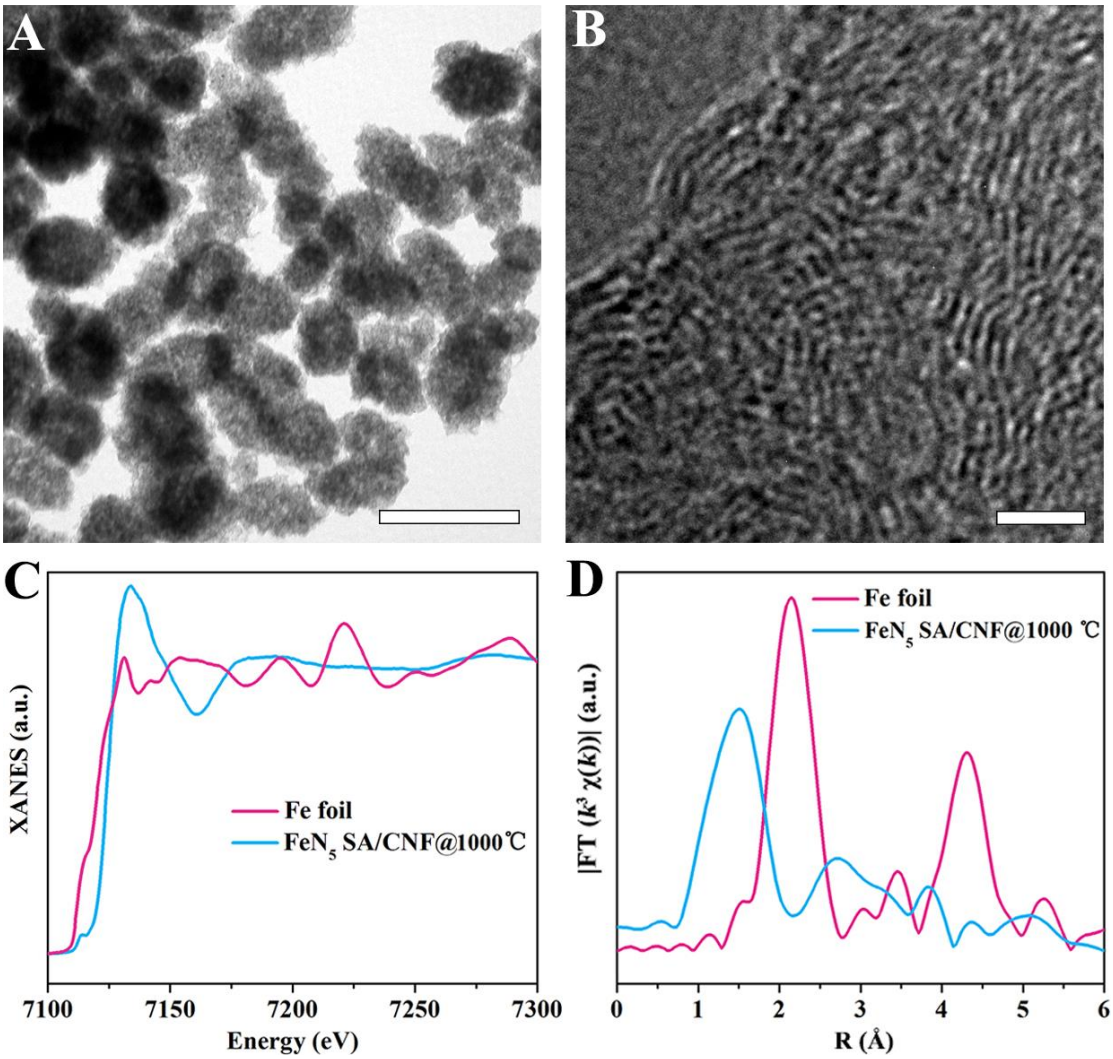

Fig. S10. Morphology and atomic structure of FeN_5 SA/CNF@1000°C. (A) TEM image and **(B)** HRTEM image of FeN_5 SA/CNF@1000 °C. **(C)** Normalized XANES spectra at Fe K-edge of the Fe foil and FeN_5 SA/CNF@1000°C, and the corresponding **(D)** k^3-weighted Fourier transform spectra. The scale bar in (A) 500 nm, (B) 2 nm.

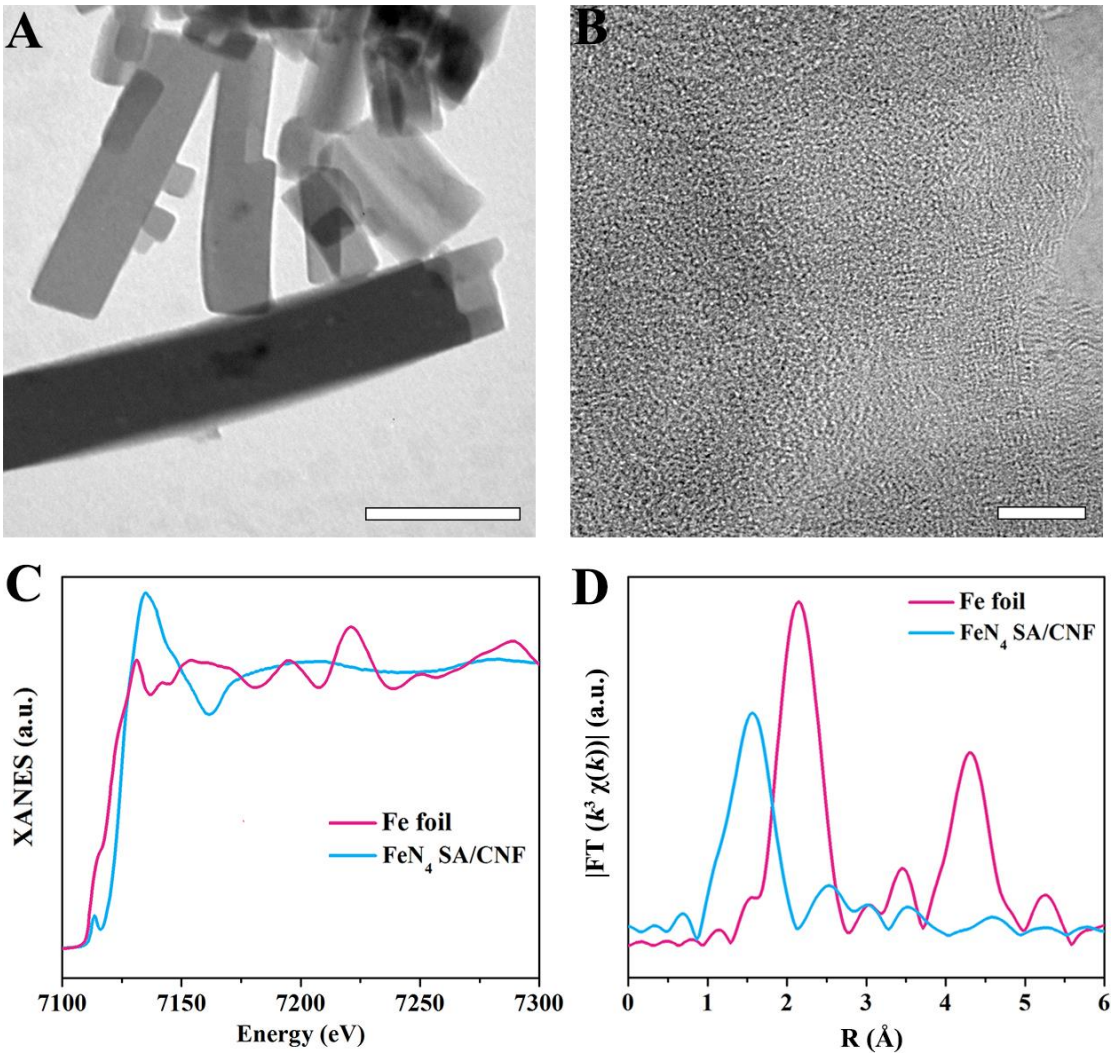

Fig. S11. Morphology and atomic structure of FeN_4 SA/CNF. (A) TEM image and **(B)** HRTEM image of FeN_4 SA/CNF. **(C)** Normalized XANES spectra at Fe K-edge of the Fe foil and FeN_4 SA/CNF, and the corresponding **(D)** k^3-weighted Fourier transform spectra. The scale bar in (A) 500 nm, (B) 5 nm.

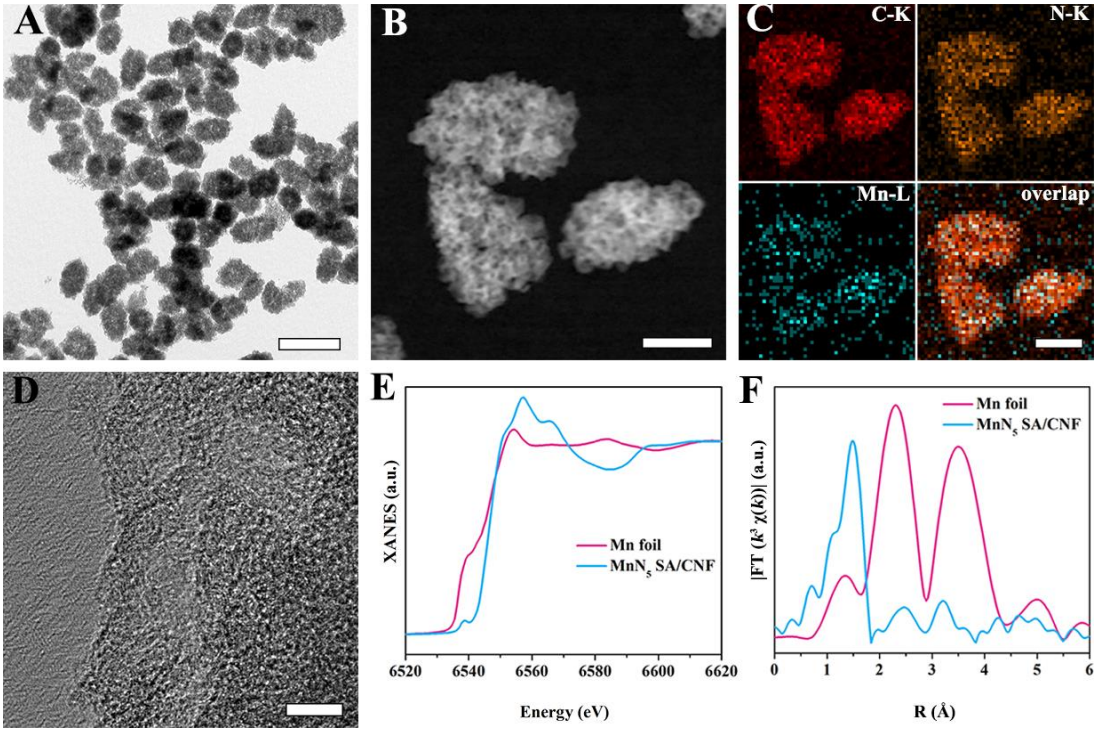

Fig. S12. Morphology and atomic structure of MnN_5 SA/CNF. (A) TEM image, **(B)** HAADF-STEM image, **(C)** TEM-EDS elemental mapping images and **(D)** HRTEM image of MnN_5 SA/CNF. **(E)** Normalized XANES spectra at Mn K-edge of the Mn foil and MnN_5 SA/CNF, and the corresponding **(F)** k^3-weighted Fourier transform spectra. The scale bar in (A) 500 nm, (B) 200 nm, (C) 200 nm and (D) 5 nm.

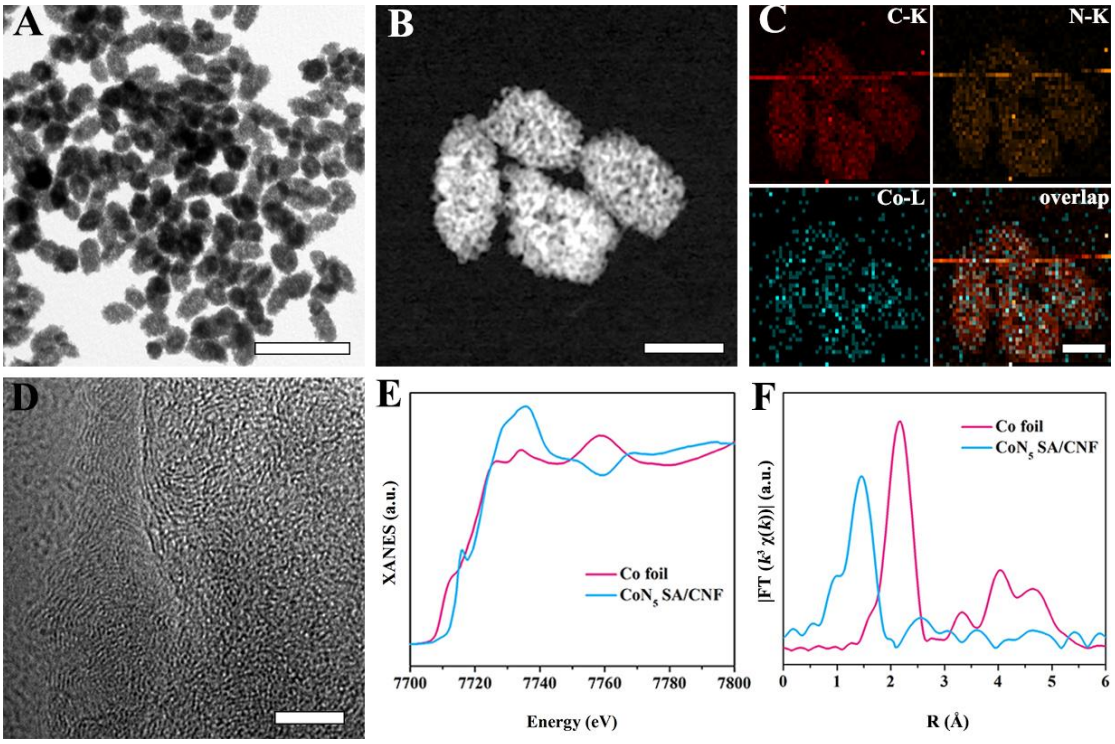

Fig. S13. Morphology and atomic structure of CoN_5 SA/CNF. (A) TEM image, **(B)** HAADF-STEM image, **(C)** TEM-EDS elemental mapping images and **(D)** HRTEM image of CoN_5 SA/CNF. **(E)** Normalized XANES spectra at Co K-edge of the Co foil and CoN_5 SA/CNF, and the corresponding **(F)** k^3-weighted Fourier transform spectra. The scale bar in (A) 1 μm, (B) 200 nm, (C) 200 nm and (D) 5 nm.

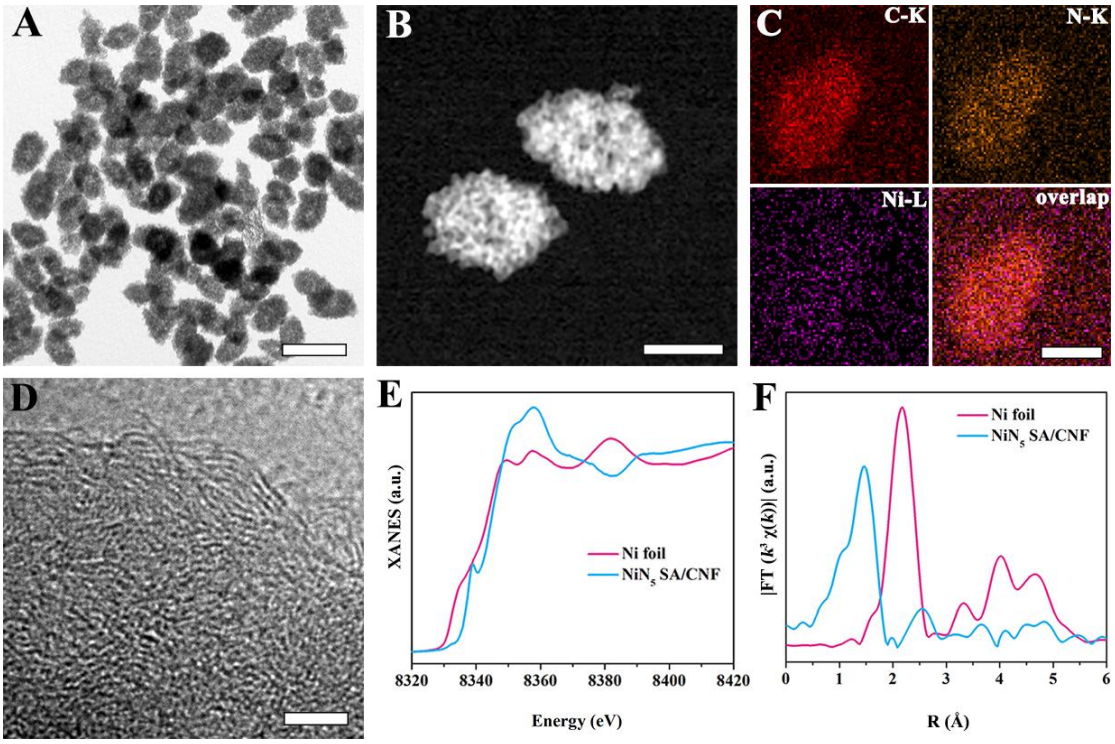

Fig. S14. Morphology and atomic structure of NiN_5 SA/CNF. (A) TEM image, **(B)** HAADF-STEM image, **(C)** TEM-EDS elemental mapping images and **(D)** HRTEM image of NiN_5 SA/CNF. **(E)** Normalized XANES spectra at Ni K-edge of the Ni foil and NiN_5 SA/CNF, and the corresponding **(F)** k^3-weighted Fourier transform spectra. The scale bar in (A) 500 nm, (B) 200 nm, (C) 200 nm and (D) 3 nm.

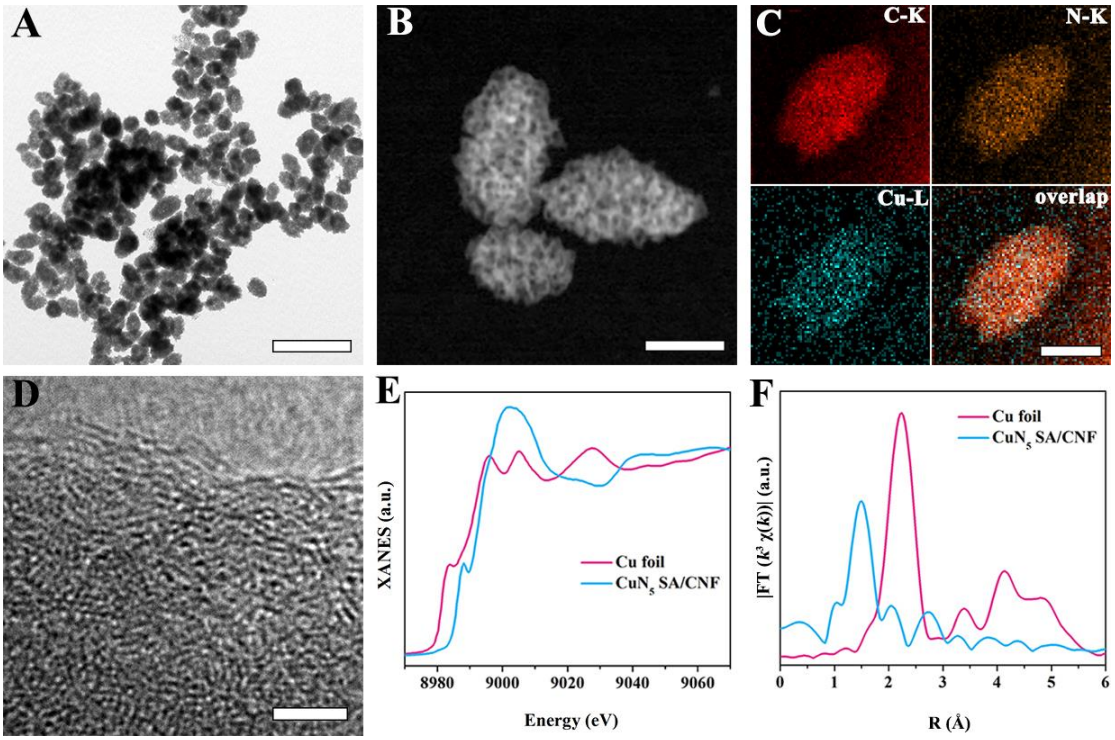

Fig. S15. Morphology and atomic structure of CuN_5 SA/CNF. (A) TEM image, **(B)** HAADF-STEM image, **(C)** TEM-EDS elemental mapping images and **(D)** HRTEM image of CuN_5 SA/CNF. **(E)** Normalized XANES spectra at Cu K-edge of the Cu foil and CuN_5 SA/CNF, and the corresponding **(F)** k^3-weighted Fourier transform spectra. The scale bar in (A) 1 μm, (B) 200 nm, (C) 200 nm and (D) 3 nm.

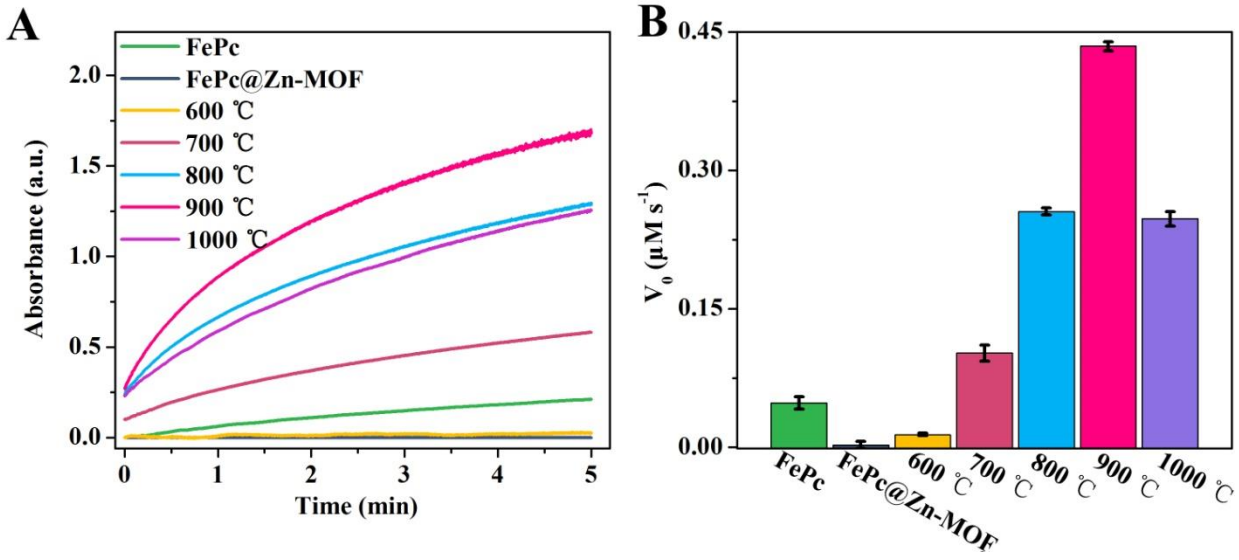

Fig. S16. UV-vis absorption spectra of the catalysts. (A) Time-dependent absorbance changes at 652 nm in the presence of FePc, FePc@Zn-MOF and FeN_5 SA/CNF obtained at different pyrolysis temperature (600°C~1000°C), and **(B)** the oxidase-like activity histogram of the corresponding catalysts.

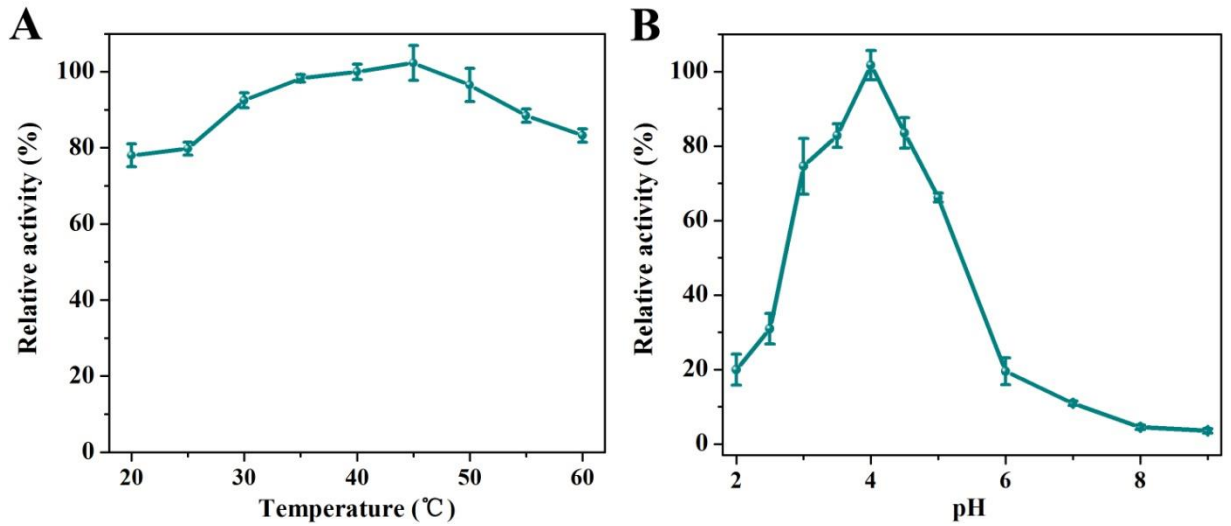

Fig. S17. Oxidase-like activities of FeN_5 SA/CNF in different conditions. (A) Temperature-dependent and **(B)** pH-dependent absorbance changes at 652 nm by using FeN_5 SA/CNF as oxidase mimics.

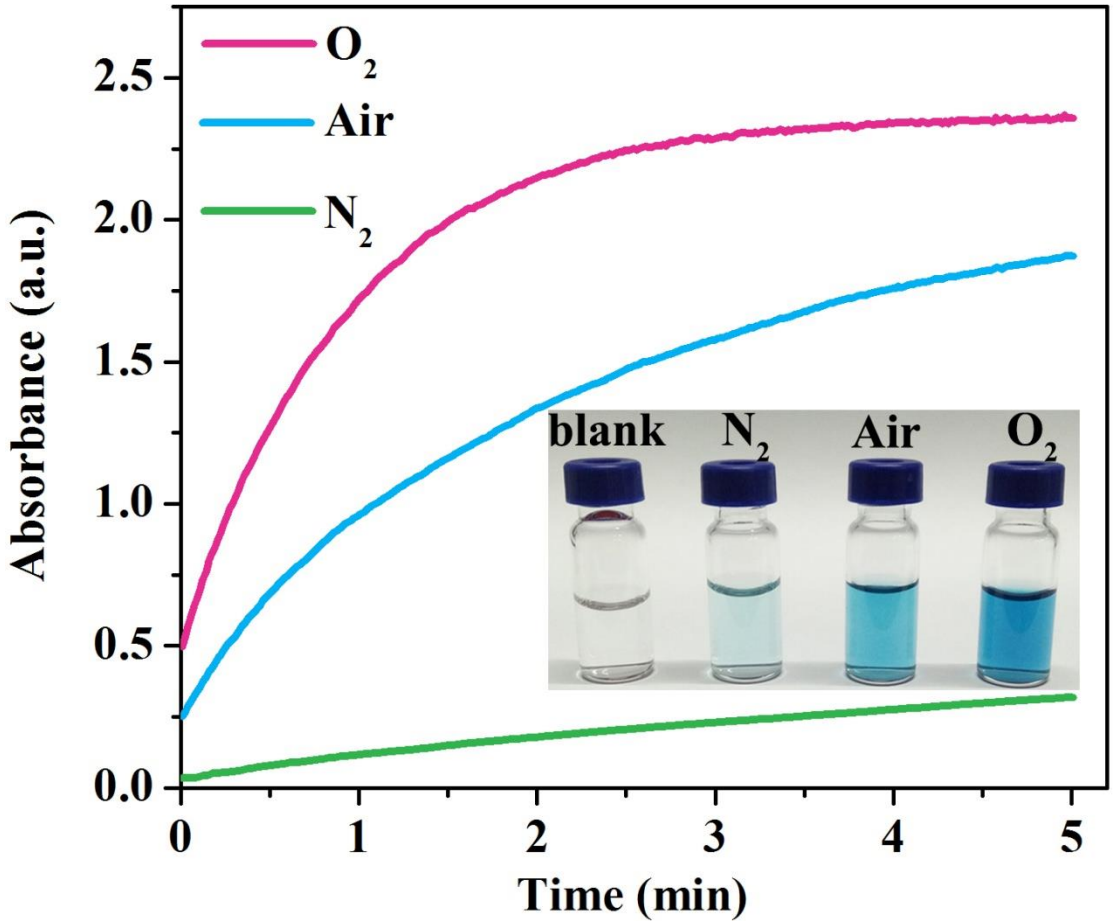

Fig. S18. UV-vis absorption spectra of FeN_5 SA/CNF. Time-dependent absorbance changes at 652 nm in the presence of FeN_5 SA/CNF in O_2- saturated, Air- saturated and N_2- saturated sodium acetate-acetic acid buffer, and the inset is an optical image of the corresponding TMB solution catalyzed by FeN_5 SA/CNF at 1 min. (Photo Credit: Liang Huang, Changchun Institute of Applied Chemistry)

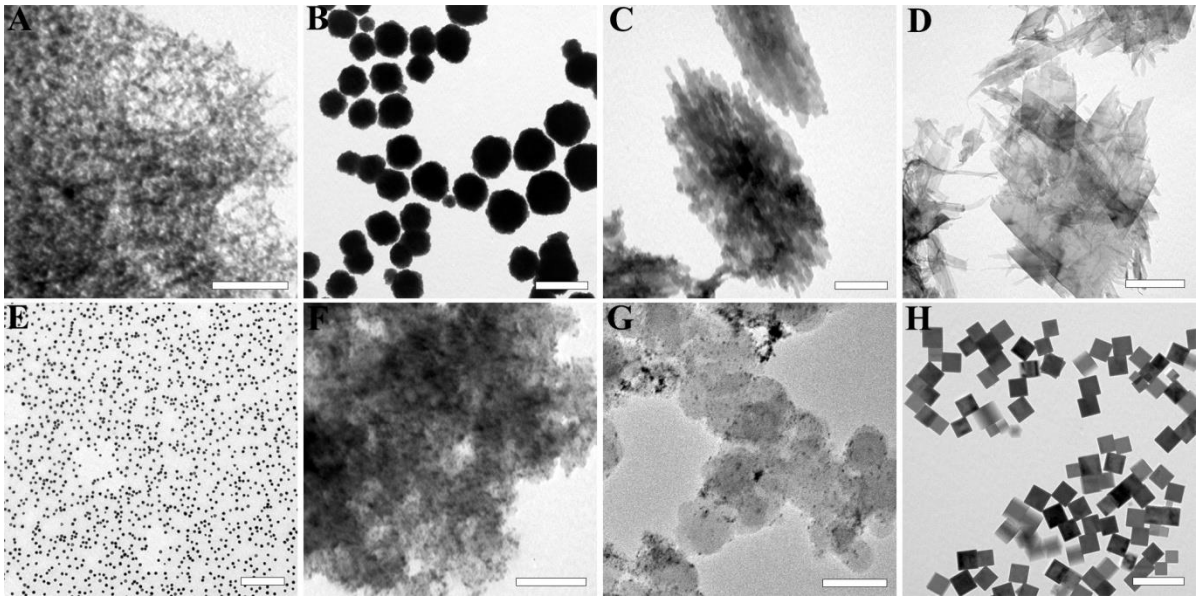

Fig. S19. Morphology and structure of synthesized conventional nanozymes. (A) MnO_2, **(B)** Fe_3O_4, **(C)** CeO_2, **(D)** CuO, **(E)** Au, **(F)** Commercial Pd/C (40%), **(G)** Commercial Pt/C (20%) and **(H)** PB. The scale bars are 100 nm, 500 nm, 200 nm, 200nm, 200 nm, 100 nm, 100 nm and 200 nm, respectively.

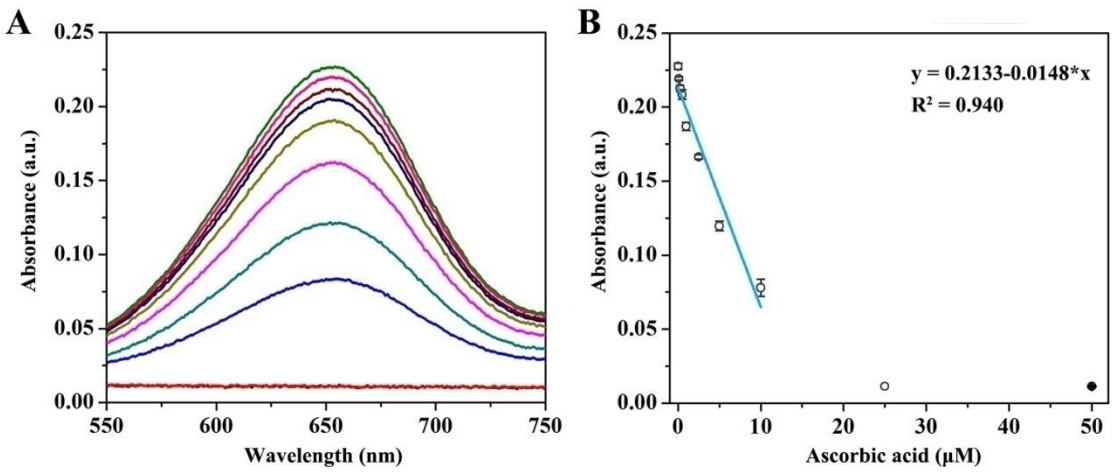

Fig. S20. UV-vis absorption spectra of TMB solutions. (A) UV-Vis absorption spectra of TMB solutions containing FeN_5 SA/CNF upon the addition of AA (0~50 μM). **(B)** Dose-response curve for AA detection at 652 nm, the error bars represent the standard deviation of four measurements. The inhibitive effect of TMB oxidation reaction by ascorbic acid (AA) makes the FeN_5 SA/CNF sensitive to the antioxidant. The oxidation rate of TMB gradually decrease with the increase of AA concentration, and there is a good linear relationship between the absorbance of oxTMB and AA concentration in the range of 0.1-10 μM with a limit of detection of 0.07 μM.

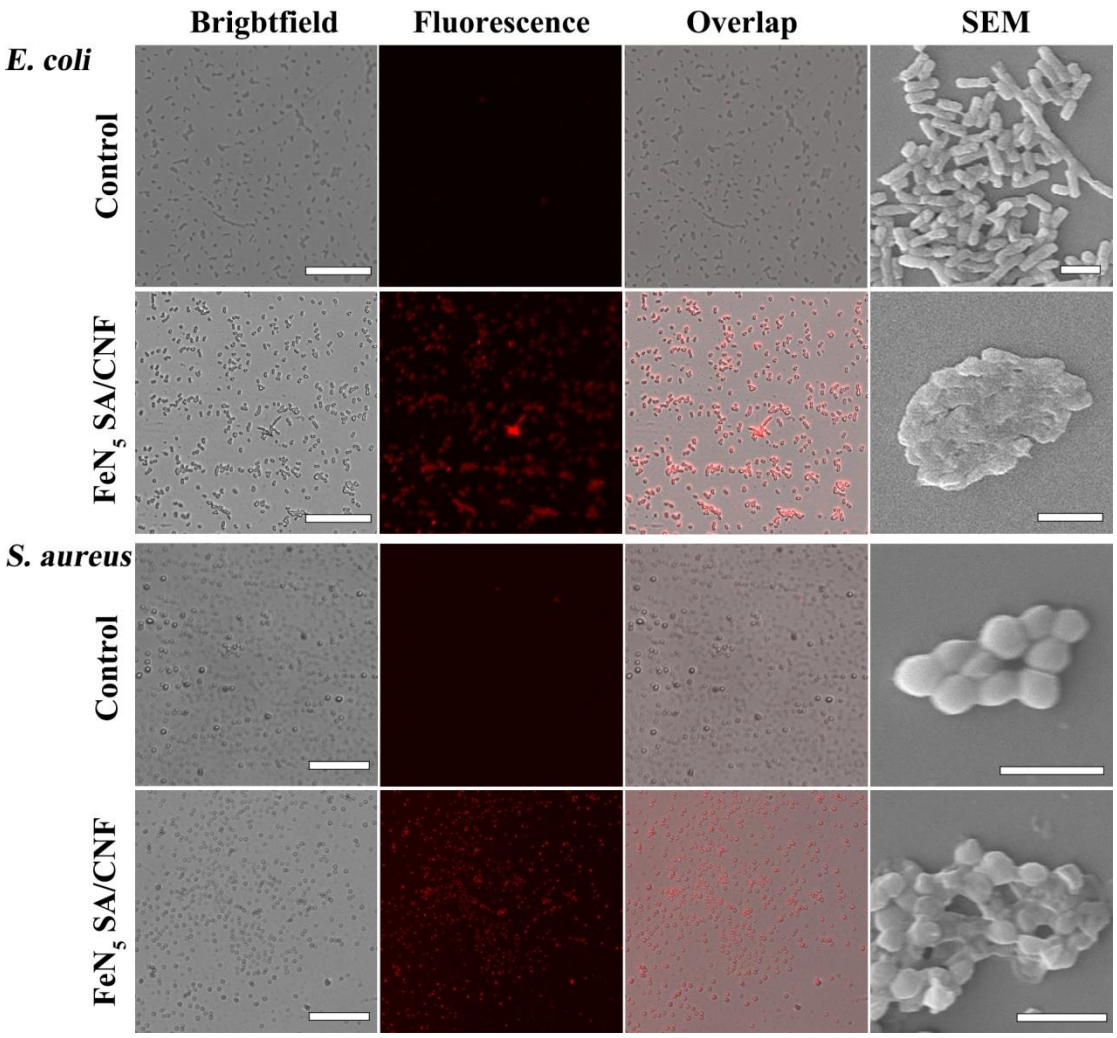

Fig. S21. Morphological changes in bacteria. Brightfield images, Fluorescence images, overlap images and SEM images of *E. coli* and *S. aureus* bacteria treated or untreated with FeN_5 SA/CNF. The scale bars are 40 μm for fluorescence images and 2 μm for SEM images.

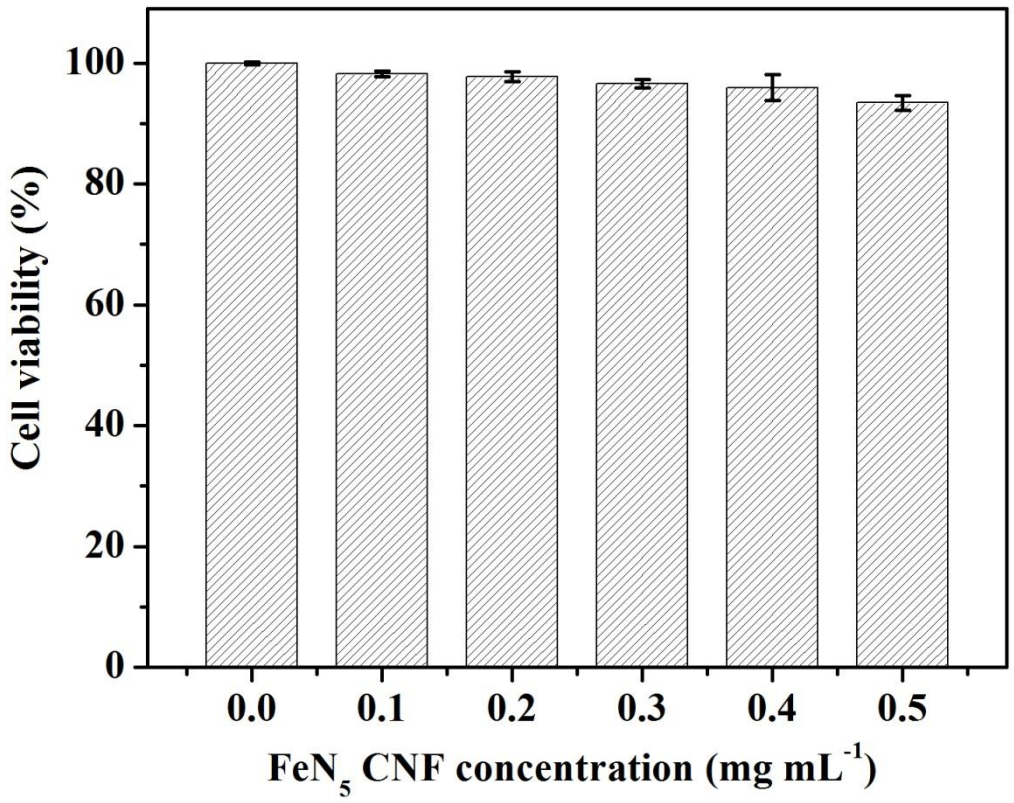

Fig. S22. In vitro cytotoxicity experiments. Cell viability of NCM460 cells after incubation with FeN_5 CNF at various concentrations (0−0.5 mg mL^{-1}) for 24 h. Values of surviving fraction are the means and standard deviation from three parallel experiments (n=8).

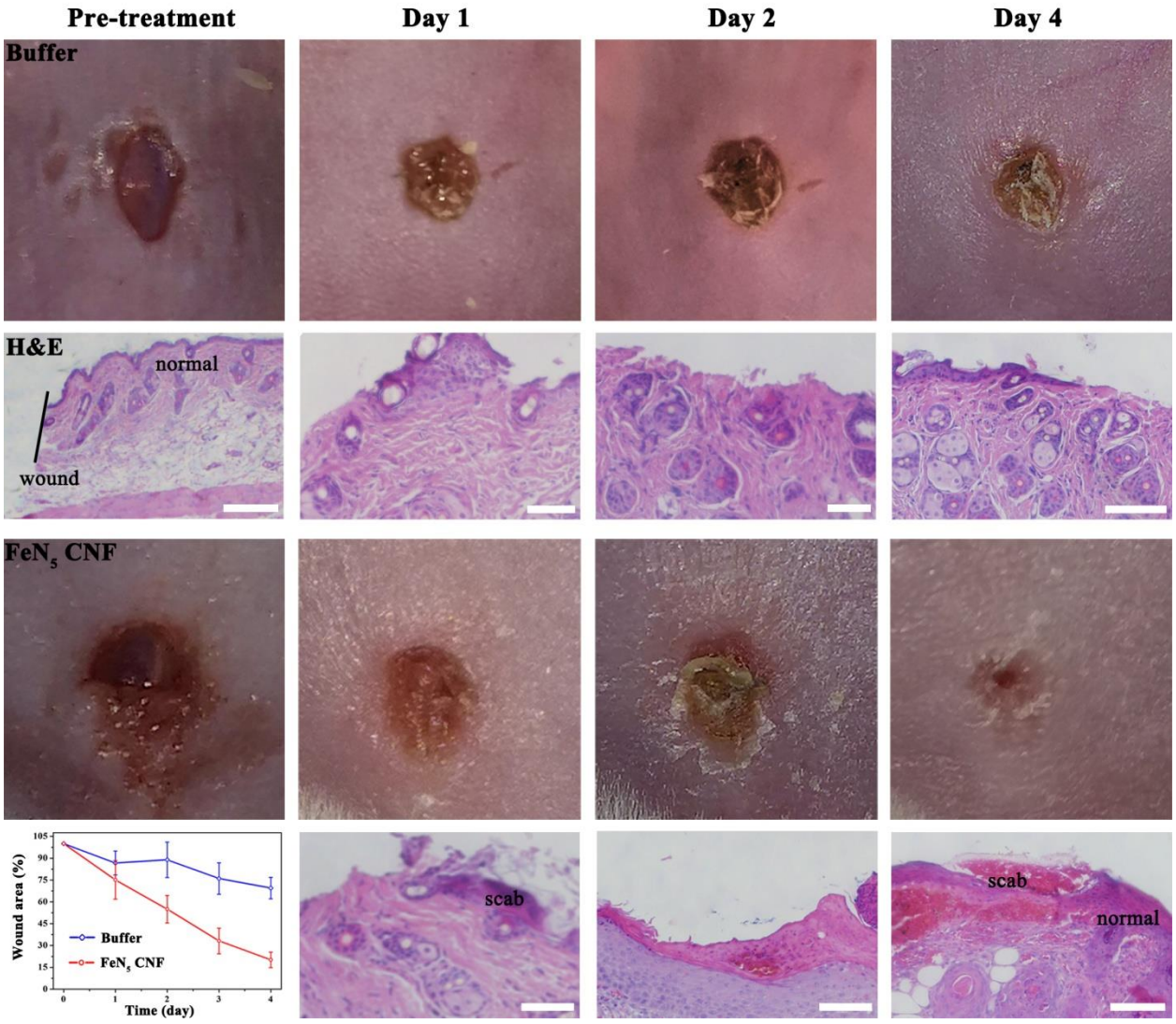

Fig. S23. Photographs of in vivo mice wound model. Photographs of *E. coli* infected wound treated with PBS buffer and FeN_5 CNF solutions at pre-treatment, the first day, the second day and the fourth day, and their corresponding histologic analyses. (Five mice in each group). Related wound size of mice in each group after different treatments (diagram in the left corner). Error bars are taken from three mice per group. The scale bars are 200 μm, 50 μm, 50 μm, 100 μm,50 μm, 100 μm and 100 μm for the H&E staining images (from left to right), respectively. (Photo Credit: Liang Huang, Changchun Institute of Applied Chemistry)

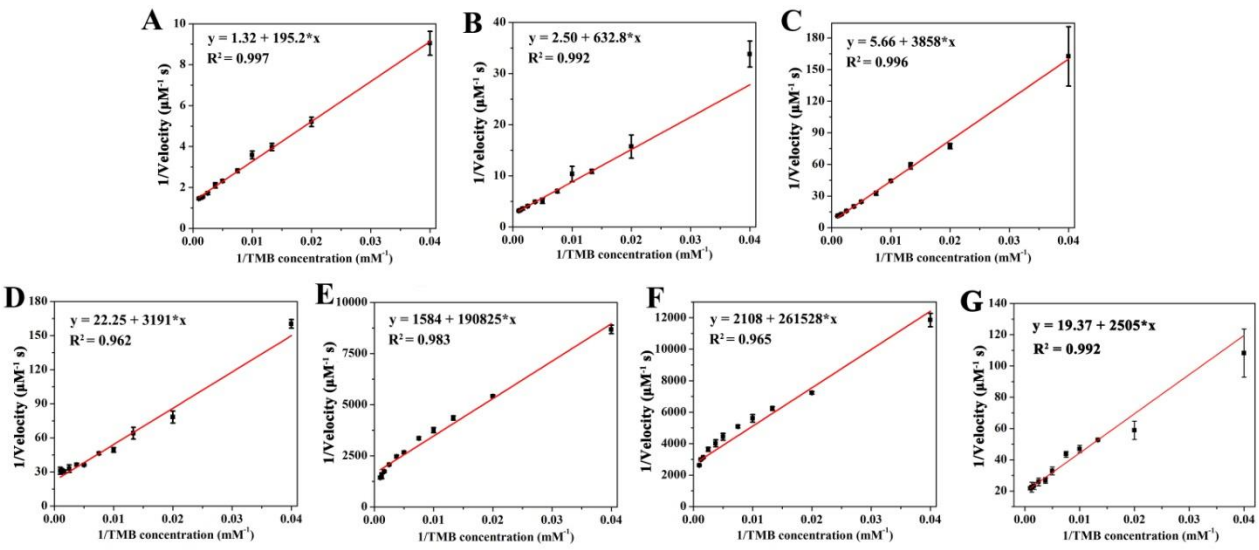

Fig. S24. Double-reciprocal plots of activity of these catalysts. (A) FeN_5 SA/CNF, **(B)** MnN_5 SA/CNF, **(C)** CoN_5 SA/CNF, **(D)** FeN_4 SA/CNF, **(E)** NiN_5 SA/CNF, **(F)** CuN_5 SA/CNF and **(G)** commercial Pt/C. The error bars represent the standard deviation of four measurements.

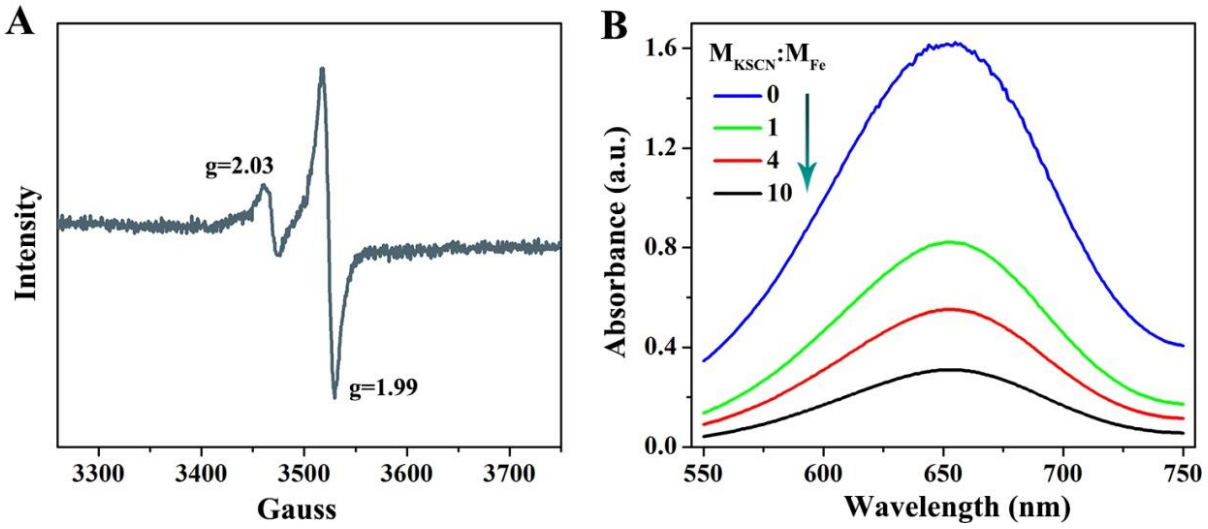

Fig. S25. The analysis of the intermediate state of and active center in FeN_5 SA/CNF. (A) X-band EPR spectrum of FeN_5 SA/CNF in acetonitrile/ PhIO at 77 K. Experimental conditions: frequency, 9.853 GHz; microwave power, 10.8 mW; center field, 3510 G; modulation amplitude, 10 G; time constant, 1.250 ms. **(B)** UV-Vis absorption spectra of TMB solutions containing FeN_5 SA/CNF upon the addition of KSCN (molar ratio of KSCN:Fe, 0~10).

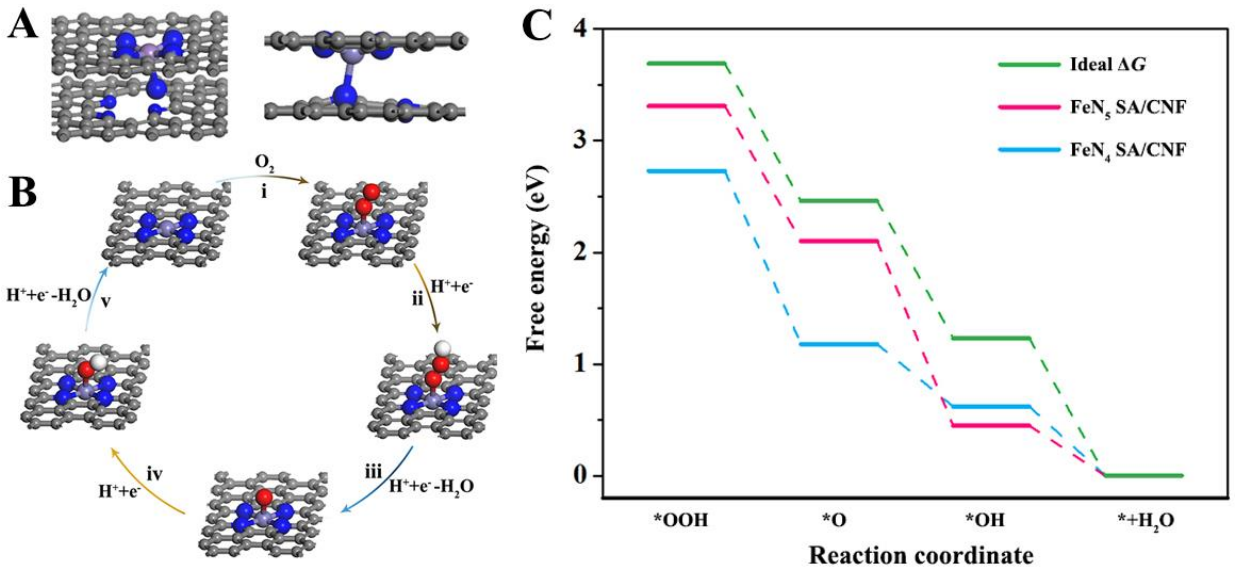

Fig. S26. Theoretical investigation of oxidase-like activity. (A) Top view and side view of FeN_5 SA/CNF theoretical model. **(B)** Proposed reaction pathways of O_2 reduction to H_2O with optimized adsorption configurations on FeN_4 SA/CNF. The gray, blue, purple, red and white balls represent the C, N, Fe, O, H atoms, respectively. **(C)** Free energy diagram of intermediate species on FeN_4 SA/CNF and FeN_5 SA/CNF compared with ideal ΔG.

Table S1. Mössbauer parameters of FeN_5 SA/CNF.

Doublet	δ_{iso}/ mm s^{-1}	ΔE_Q/ mm s^{-1}	Area/ %
D1	0.24	0.82	58.57
D2	0.13	2.75	24.65
D3	0.26	1.34	16.78

Table S2. Comparison of oxidase-like activity of synthesized catalysts.

Catalysts	MnO_2	Fe_3O_4	CeO_2	CuO	Au	Pd/C	Pt/C	PB
v_0/μM s^{-1}	0.0496	0.0009	0.0036	0.0001	0.0011	0.0038	0.0454	0.0002
[E]/μM	57.47	64.66	29.07	62.89	25.38	18.86	5.13	35.71
k_{cat}'/10^{-3} s^{-1}	0.863	0.014	0.124	0.002	0.043	0.201	8.850	0.006

k_{cat}' is the catalytic constant, which is normalized the initial reaction velocity with [E] at standard conditions (air-saturated 0.4 mM TMB solution), $k_{cat}' = v_0/[E]$, [E] is the molar concentration of metal in nanozymes.

Table S3. Comparison of the kinetic constants of the single-atom enzyme mimics.

Catalysts	K_m (mM)	v_{max} (μM s^{-1})	k_{cat} (10^{-1} s^{-1})	k_{cat}/K_m (mM^{-1} s^{-1})
FeN_5 SA/CNF	0.148	0.758	7.084	4.787
MnN_5 SA/CNF	0.253	0.400	3.740	1.478
CoN_5 SA/CNF	0.682	0.177	1.743	0.256
FeN_4 SA/CNF	0.143	0.045	0.421	0.296
NiN_5 SA/CNF	0.120	6×10^{-4}	0.006	0.005
CuN_5 SA/CNF	0.124	4.7×10^{-4}	0.005	0.004
Commercial Pt/C	0.129	0.052	0.101	0.079

K_m is the Michaelis constant, v_{max} is the maximal reaction velocity and k_{cat} is the catalytic constant, where $k_{cat} = v_{max}/[E]$, [E] is the molar concentration of metal in nanozymes.

Table S4. The adsorption energy on the single-atom catalysts.

Free energy (eV)	ΔG_{*O_2}	$\Delta G_{*O_2\text{-}*OOH}$
FeN_4 SA/CNF	0.05	2.19
CoN_5 SA/CNF	0.45	0.85
MnN_5 SA/CNF	0.39	0.73
FeN_5 SA/CNF	0.79	0.82

Table S5. Reaction free energy of intermediate species on single-atom catalysts.

Free energy (eV)	FeN_4 SA/CNF	CoN_5 SA/CNF	MnN_5 SA/CNF	FeN_5 SA/CNF
$*O_2$	4.87	4.47	4.53	4.13
*OOH	2.73	3.62	3.80	3.31
*O	1.18	2.87	2.18	2.10
*OH	0.62	0.72	0.75	0.45

Table S6. Comparison of the kinetic constants of FeN_5 SA/CNF and nanozymes.

Catalysts	K_m (mM)	v_{max} ($\mu M\ s^{-1}$)	k_{cat} ($10^{-1}\ s^{-1}$)	k_{cat}/K_m ($mM^{-1}\ s^{-1}$)	Ref
FeN_5 SA/CNF	0.148	0.758	7.08	4.786	This work
Nano-CeO_2	0.420	0.100	0.02	0.005	*(44)*
Ce-MOF [a]	0.088	0.110	0.013	0.011	*(45)*
Mn_3O_4 NPs [b]	0.025	0.051	0.005	0.0204	*(46)*
Co_3Fe LCC-LDH [c]	0.050	0.387	0.013	0.0267	*(47)*
Fe/NC-800	0.170	0.089	0.002	0.0012	*(48)*
Au@HCNs [d]	0.170	0.049	0.043	0.0256	*(49)*
MSN-AuNPs [e]	0.225	0.118	0.297	0.132	*(34)*
Ru NPs	54.92	0.010	2×10^{-4}	3.5×10^{-7}	*(50)*
Pt NPs	0.051	0.109	0.072	0.141	*(51)*
N-PCNSs-5 [f]	0.095	0.003	−	−	*(7)*

K_m is the Michaelis constant, v_{max} is the maximal reaction velocity and k_{cat} is the catalytic constant, where $k_{cat} = v_{max}/[E]$, [E] is the molar concentration of metal in nanozymes.

[a] MOF: Metal-organic framework; [b] NPs: Nanoparticles;

[c] LCC-LDH: Lyotropic liquid crystals -layered double hydroxides;

[d] HCNs: Hollow carbon nanospheres; [e] MSN: Mesoporous silica;

[f] N-PCNSs: N-doped porous carbon nanospheres.